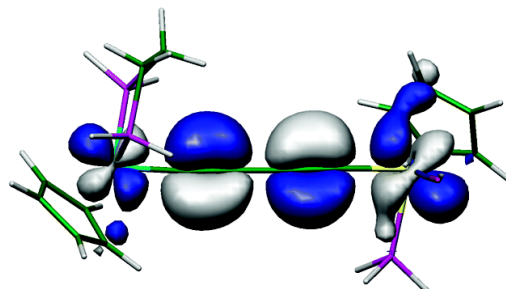# J|A|C|S
JOURNAL OF THE AMERICAN CHEMICAL SOCIETY

Article

Bonding and Electronic Structure in Consanguineous and Conjugal Iron and Rhenium sp Carbon Chain Complexes [MCM']: Computational Analyses of the Effect of the Metal

Haijun Jiao, Karine Costuas, John A. Gladysz, Jean-Franois Halet, Maud Guillemot, Loic Toupet, Frdric Paul, and Claude Lapinte

HOMO of $(\eta^5\text{-}C_5H_5)(\eta^2\text{-}H_2PCH_2CH_2PH_2)FeC_4Re(PH_3)(NO)(\eta^5\text{-}C_5H_5)$

More About This Article

Additional resources and features associated with this article are available within the HTML version:

- Supporting Information
- Links to the 14 articles that cite this article, as of the time of this article download
- Access to high resolution figures
- Links to articles and content related to this article
- Copyright permission to reproduce figures and/or text from this article

View the Full Text HTML

ACS Publications
High quality. High impact.

Bonding and Electronic Structure in Consanguineous and Conjugal Iron and Rhenium sp Carbon Chain Complexes [MC$_4$M']$^{n+}$: Computational Analyses of the Effect of the Metal

Haijun Jiao,[†,‡] Karine Costuas,[‡] John A. Gladysz,*[†] Jean-François Halet,*[‡]
Maud Guillemot,[§] Loic Toupet,[||] Frédéric Paul,[§] and Claude Lapinte[§]

*Contribution from the Institut für Organische Chemie, Friedrich-Alexander-Universität
Erlangen-Nürnberg, Henkestrasse 42, 91054 Erlangen, Germany, Laboratoire de Chimie du
Solide et Inorganique Moléculaire, UMR CNRS 6511, Organométalliques et Catalyse, UMR
CNRS 6509 of the Institut de Chimie de Rennes, and Groupe Matière Condensée et Matériaux,
UMR CNRS 6626, Université de Rennes 1, 35042 Rennes, France*

Received February 12, 2003; E-mail: gladysz@organik.uni-erlangen.de; halet@univ-rennes1.fr

Abstract: Density functional theory has been used to probe the bonding and electronic properties of the homo- and heterobimetallic sp carbon chain complexes [L$_m$MC$_4$M'L$_n'$]$^{z+}$ (ML$_m$, M'L$_n'$ = (η^5-C$_5$R$_5$)(η^2-R$_2$-PCH$_2$CH$_2$PR$_2$)Fe, (η^5-C$_5$R$_5$)(NO)(PR$_3$)Re; z = 0−4). All neutral complexes are best described by MC≡CC≡CM electronic structures, in accord with much experimental data. The singlet dications are best described by cumulenic $^+$M=C=C=C=C=M$^+$ valence formulations. However, the diiron and rhenium/iron dications are found to possess triplet states of nearly identical energy, clarifying experimental magnetic data. Their electronic structures have dominant $^{•+}$MC≡CC≡CM$^{+•}$ character, with some spin delocalization onto the carbon chain. The mixed valence monocation radicals exhibit delocalized unpaired electrons, in accord with class III (strongly coupled) and II (weakly coupled) assignments made from experimental data earlier, with some spin density on the carbon chain. An isolable diiron trication has a doublet ground state, but some computational data suggest a close-lying quartet. For the unknown diiron tetracation, a bis-(carbyne) or $^{2+}$Fe≡CC≡CC≡CFe^{2+} electronic structure is predicted. Calculated adiabatic ionization potentials show the iron endgroup to be more electron-releasing than rhenium, in accord with electrochemical data. This polarizes the electronic structures of the rhenium/iron complexes. To help validate the computed model structures, crystal structures of {(η^5-C$_5$Me$_5$)Fe(η^2-dppe)}$_2$(μ-C$_4$) and [{(η^5-C$_5$Me$_5$)Fe(η^2-dippe)}$_2$(μ-C$_4$)]$^{3+}$ 3PF$_6^-$ are determined. Data are analyzed with respect to related diruthenium and dimanganese complexes.

Introduction

Long range electronic, magnetic, and charge communication between metallic centers represent cornerstones of molecular electronics. The control and manipulation of such interactions is of immense practical and theoretical importance. Complexes in which two transition metal fragments that differ by a single electron are bridged by fully conjugated, unsaturated organic ligands have been known since the discovery of the Creutz−Taube ion, [(H$_3$N)$_5$Ru−NC$_4$H$_4$N−Ru(NH$_3$)$_5$]$^{5+}$.[1] Such mixed-valence species, which undergo facile intramolecular electron transfer between the redox active metal centers,[2] have been viewed as attractive building blocks for molecular electronics. Many compounds have been tested in this capacity, with studies focusing both on the role of the metal centers and on the

influence of the conjugated ligands[3] as electron-conductive fragments to promote long-range interactions between two metal termini.

Among these bridges, wirelike or one-dimensional conjugated carbon chains consisting of as many as 20 atoms[4] have received considerable attention. There has been speculation that such assemblies, L$_m$MC$_x$M'L$_n$, would be well suited for nonlinear optics and molecular devices such as switches and wires.[5] Carbon chain ligands are particularly novel in their valence flexibility, as they are able to form single (M−C), double (M=C), and triple (M≡C) bonds to metals. For complexes with even-numbered carbon chains, three limiting valence structures can

---

† Institut für Organische Chemie.
‡ Laboratoire de Chimie du Solide et Inorganique Moléculaire.
§ Organométalliques et Catalyse.
|| Groupe Matière Condensée et Matériaux.

(1) (a) Creutz, C.; Taube, H. *J. Am. Chem. Soc.* **1973**, *95*, 1086. (b) Demadis, K. D.; Hartshorn, C. M.; Meyer, T. J. *Chem. Rev.* **2001**, *101*, 2655 and earlier reviews cited therein.
(2) Taube, H. *Angew. Chem.* **1984**, *96*, 315; *Angew. Chem., Int. Ed. Engl.* **1984**, *23*, 329 and references therein.

(3) (a) Ward, M. D. *Chem. Soc. Rev.* **1995**, 121, and references therein. (b) McCleverty, J. A.; Ward, M. D. *Acc. Chem. Res.* **1998**, *31*, 842.
(4) (a) Dembinski, R.; Bartik, T.; Bartik, B.; Jaeger, M.; Gladysz, J. A. *J. Am. Chem. Soc.* **2000**, *122*, 810. (b) Bartik, T.; Bartik, B.; Brady, M.; Dembinski, R.; Gladysz, J. A. *Angew. Chem.* **1996**, *108*, 467, *Angew. Chem., Int. Ed. Engl.* **1996**, *35*, 414.
(5) (a) Schwab, P. F.; Levin, M. D.; Michl, J. *Chem. Rev.* **1999**, *99*, 1863. (b) Bunz, U. H. F. *Angew. Chem.* **1996**, *108*, 1047; *Angew. Chem., Int. Ed. Engl.* **1996**, *35*, 968. (c) Lang, H. *Angew. Chem.* **1994**, *106*, 569; *Angew. Chem., Int. Ed. Engl.* **1994**, *33*, 547. (d) Long, N. J. *Angew. Chem.* **1995**, *107*, 37; *Angew. Chem., Int. Ed. Engl.* **1995**, *34*, 21. (e) Beck, W.; Niemer, B.; Wieser, M. *Angew. Chem.* **1993**, *105*, 969; *Angew. Chem., Int. Ed. Engl.* **1993**, *32*, 923. (f) Paul, F.; Lapinte, C. In *Unusual Structures and Physical Properties in Organometallic Chemistry*; Gielen, M., Willem, R., Wrackmeyer, B., Eds.; Wiley: New York, 2002; pp 220−291. (g) Paul, F.; Lapinte, C. *Coord. Chem. Rev.* **1998**, *178−180*, 431.

Scheme 1. Some Possible Valence Structures for Carbon Ligands Bridging Two Metal Centers
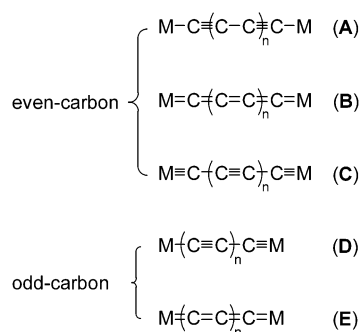
Scheme 2. Possible Redox States for Even-Numbered Carbon Complexes[a]
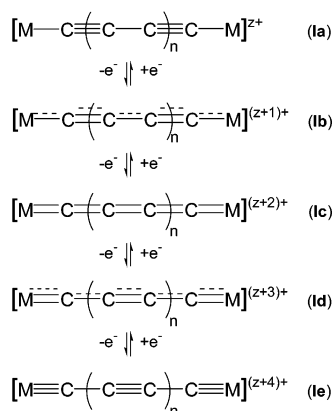
[a] For additional possibilities regarding electronic structures, see Scheme 4.

be written (Scheme 1, **A**−**C**). Structures **A** and **C** are based upon polyynes with alternating single and triple bonds, whereas **B** is a fully double-bonded cumulenic system. With odd-numbered carbon chains, both polyyne and cumulenic valence structures involving at least one M−C multiple bond are possible (Scheme 1, **D** and **E**).

Most neutral, even-carbon-chain complexes prepared to date feature the polyyne valence structure **A**. However, examples with structural patterns **B** and **C** have also been reported, for example, $(Bu^tSiO)_3Ta=C=C=Ta(OSiBu^t)_3$[6] and $(Bu^tO)_3W\equiv$ $C-C\equiv W(OBu^t)_3$.[7] Valence structures **B** and **C** can also be generated by two-electron oxidations of **A** as shown in Scheme 2 (**Ia** → **Ic** → **Ie**). In some cases, intermediate oxidation states have been characterized (**Ib**, **Id**), and examples are analyzed in detail below. These represent, like the Creutz−Taube ion, mixed valence compounds. Such series of redox-related species have been termed "consanguineous" and, in the case of unlike endgroups, "conjugal".[8]

Among all of these complexes, tetracarbon species $L_mMC_4M'L'_n$ have been the most intensively investigated, both experimentally and theoretically. Some representative examples are shown in Scheme 3 (**1**−**5**). With the iron and chiral rhenium endgroups $(\eta^5\text{-}C_5Me_5)Fe(\eta^2\text{-dppe})$ (dppe = $Ph_2PCH_2CH_2PPh_2$)

Scheme 3. Representative MC_4M Complexes
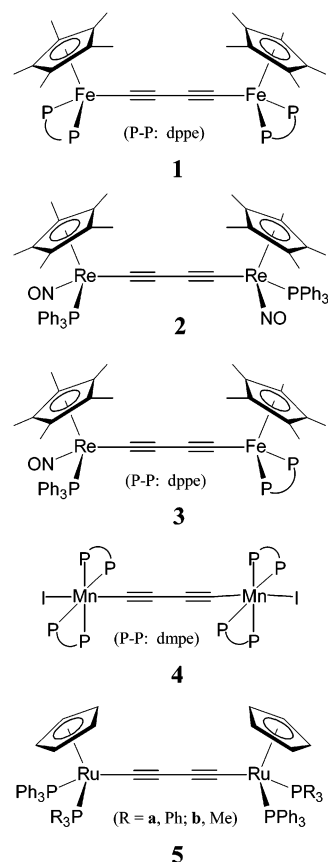
and $(\eta^5\text{-}C_5Me_5)Re(NO)(PPh_3)$, families of homo- (**1, 2**)[8,9] and heterobimetallic (**3**) adducts have been isolated.[10] All undergo two reversible single-electron oxidations, evidenced by cyclic voltammetry, and exhibit strong interactions between the metal centers, as indicated by the large differences between their first two redox potentials [$\Delta E° = 0.72$ (**1**); 0.53 (**2**); 0.73 V (**3**)]. Chemical oxidations give isolable cation radicals $[1-3]^+ PF_6^-$ and dications $[1-3]^{2+} 2PF_6^-$ that are stable at room temperature. Products derived from the further oxidation of **2** and **3** have not so far been observed. On the other hand, the trication 1^{3+} $3PF_6^-$ can be detected by cyclic voltammetry.[11] When the dppe ligand is substituted by the more electron-releasing isopropyl-substituted dippe ligand, $[\{(\eta^5\text{-}C_5Me_5)Fe(\eta^2\text{-dippe})\}_2(\mu\text{-}C_4)]^{3+}$ (6^{3+} $3PF_6^-$) can be isolated.[11]

1,3-Butadiynediyl or $MC\equiv CC\equiv CM$ electronic structures (**A**) best describe the neutral species **1**−**3**, as clearly indicated by various data reviewed below.[8−10] However, a variety of questions accompany the other oxidation states, which we seek to address by computational means in this paper, particularly with regard to the influence of the metal. For example, which valence structure best describes the unsymmetrical conjugal cation radical $3^+ PF_6^-$? Similarly, with the dications $[1-3]^{2+} 2PF_6^-$, singlet (**S**) and triplet (**T**) spin states are possible,[12] limiting formulations of which are exemplified with **Ic** in Scheme 4.

(6) Neithamer, D. R.; LaPointe, R. E.; Wheeler, R. A.; Richeson, D. S.; Van Duyne, G. D.; Wolczanski, P. T. *J. Am. Chem. Soc.* **1989**, *111*, 9056.

(7) (a) Caulton, K. G.; Cayton, R. H.; Chisholm, R. H.; Huffman, J. C.; Lobkovsky, E. B.; Xue, Z. *Organometallics* **1992**, *11*, 321. (b) Listemann, M. L.; Schrock, R. R. *Organometallics* **1985**, *4*, 74.

(8) Brady, M.; Weng, W.; Zhou, Y.; Seyler, J. W.; Amoroso, A. J.; Arif, A. M.; Böhme, M.; Frenking, G.; Gladysz, J. A. *J. Am. Chem. Soc.* **1997**, *119*, 775.

(9) (a) Le Narvor, N.; Toupet, L.; Lapinte, C. *J. Chem. Soc., Chem. Comm.* **1993**, 357. (b) Le Narvor, N.; Toupet, L.; Lapinte, C. *J. Am. Chem. Soc.* **1995**, *117*, 7129.

(10) Paul, F.; Meyer, W.; Toupet, L.; Jiao, H.; Gladysz, J. A.; Lapinte, C. *J. Am. Chem. Soc.* **2000**, *122*, 9405.

(11) Guillemot, M.; Toupet, L.; Lapinte, C. *Organometallics* **1998**, *17*, 1928. The Z-value was incorrectly reported in Table 1 of the Supporting Information. Z = 2.

(12) Le Narvor, N.; Lapinte, C. *C. R. Acad. Sci.* **1998**, T1, Ser. IIc, 745.

Scheme 4. Additional Formulations for Some of the Redox States in Scheme 2, Illustrated for $n = 1$ (C₄ bridge) and $z = 0$

M—C≡C—C≡C—M ⇌ M—C≡C—C≡C—M

M=C=C=C=C—M or M—C=C=C=C=M

M=C=C—C≡C—M M—C≡C—C=C=M

Ib

M—C=C=C=C=M   **Ic-(S)**

spin ‖ equilbrium

M—C≡C—C≡C—M   **Ic-(T)**

M=C=C=C—C≡C—M ⟷ M—C≡C—C=C=C—M

M=C=C—C≡C—M ⟷ M—C≡C—C=C=M

M=C=C=C=C—M ⟷ M—C=C=C=C=M

M—C=C—C≡C—M ⟷ M—C≡C—C—C=M   **Id-(D)**

M=C=C=C=C—M ⟷ M—C=C=C=C=M

(and others)

spin ‖ equilbrium

M—C=C—C≡C—M ⟷ M—C≡C—C=C—M   **Id-(Q)**

M—C≡C—C=C—M ⟷ M—C≡C—C=C—M

(and others)
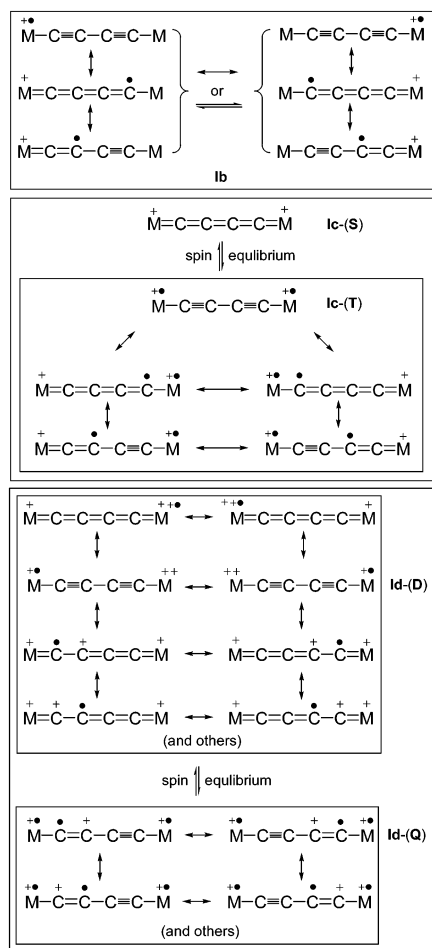
Trications such as $\mathbf{1}^{3+}$ 3PF₆⁻ and $\mathbf{6}^{3+}$ 3PF₆⁻ might possess either doublet (**D**) or quartet (**Q**) states with one and three unpaired electrons, respectively, as shown for **Id**.[5f]

Some related studies merit note at the outset. First, Berke has synthesized the dimanganese complex **4** and the oxidation products **4⁺** PF₆⁻ and **4²⁺** 2PF₆⁻.[13] In contrast to the other examples in Scheme 3, the endgroups in **4** carry only 17 valence electrons. Unique properties of these systems are discussed below. The diruthenium complexes **5** have been extensively studied by Bruce and Low.[14] These undergo four stepwise single-electron oxidations, spanning the entire range represented in Scheme 2, as assayed by cyclic voltammetry. The mono- and dications have been isolated, and the tri- and tetracations spectroscopically characterized. Since the endgroups in **5** are essentially isostructural or isoelectronic with those in **1** and **2**, key properties are described with our data below. Finally, Ren has shown that in [Ru₂]C₄[Ru₂] systems, which feature coordinatively unsaturated *bi*metallic termini, six oxidation states can be accessed.[15] Two are derived by reduction of the redox state analogous to **Ia** (Scheme 2) and three by oxidation.[16]

On the computational side, Sgamellotti has studied the model compounds $[\{(\eta^5\text{-}C_5H_5)(CO)_2M\}_2(\mu\text{-}C_x)]$ (M = Cr, Mn, Fe; x = 2, 4, 6, 8) by density functional theory (DFT).[17,18] Structure and bonding was evaluated as a function of metal, chain length, oxidation state, and dⁿ-configuration.[17] Some of the present authors have similarly investigated the diruthenium complexes $[\{(\eta^5\text{-}C_5H_5)(PH_3)_2Ru\}_2(\mu\text{-}C_4)]^{n+}$ ($n = 0–4$; [**5-H**]ⁿ⁺), which are models for Bruce's systems.[14,19] Key data are integrated with the new results below. In other relevant work, Frenking has described Hartree−Fock studies of the dirhenium complexes $[\{(Cl)(NO)(PH_3)Re\}_2(\mu\text{-}C_4)]^{n+}$ ($n = 0–2$), which are models for $\mathbf{2}^{n+}$ nPF₆⁻.[8] However, the cation radical ($n = 1$) did not give SCF convergence. Homo- and heterobimetallic C₃, C₅, C₇, and C₉ complexes with various combinations of $(\eta^5\text{-}C_5H_5)(NO)$-$(PH_3)Re$, $(\eta^5\text{-}C_5H_5)(CO)_2M$ (M = Mn, Re), and $(MeO)_3W$ endgroups have also been investigated.[20]

In this paper, we apply a variety of DFT computational methods to questions of bonding and electronic structure in the diiron, dirhenium, and iron/rhenium complexes $[\mathbf{1}–\mathbf{3}]^{n+}$ nPF₆⁻. The data provide particular insight regarding various marked differences between these series of compounds, and also the related diruthenium species $\mathbf{5}^{n+}$ nPF₆⁻. They are especially useful in cases where experimental observations do not unequivocally distinguish between two limiting possibilities. Also, some new structural data are reported. The net result is a consistent and comprehensive bonding model for these three series of consanguineous complexes that rationalizes the effect of the metal and accounts for all observable properties.

Results and Discussion

1. New Structural Data. To best interpret the computational results below, structural data are needed for as many oxidation states as possible. To address a conspicuous gap, crystals of **1** were obtained as described in the Experimental Section, and the X-ray structure was determined. Key data are given in Tables 1 and 2, and the molecular structure is shown in Figure 1 (top). As expected from many earlier structures of related monocyclopentadienyl complexes, the iron endgroups exhibit formally octahedral geometries,[9,21,22] with bond lengths and angles in previously established ranges.[10]

Various data in Table 2 are relevant to results below. For example, the iron−C(sp) or Fe−C$_\alpha$≡ bonds (1.884(2) Å and 1.889(2) Å) are shorter than analogous iron−C(sp³) bonds (2.003(4) Å in $[(\eta^5\text{-}C_5Me_5)(\eta^2\text{-dppe})(CHOMe)]^+$ PF₆⁻ for instance).[23] The oxidized congener **1⁺** PF₆⁻ exhibits moderately different bond lengths and angles within the FeC₄Fe core,[9] in

(13) Kheradmandan, S.; Heinze, K.; Schmalle, H. W.; Berke, H. *Angew. Chem.* **1999**, *111*, 2412; *Angew. Chem., Int. Ed.* **1999**, *38*, 2270.
(14) Bruce, M. I.; Low, P. J.; Costuas, K.; Halet, J.-F.; Best, S. P.; Heath, G. A. *J. Am. Chem. Soc.* **2000**, *122*, 1949.
(15) Ren, T.; Zou, G.; Alvarez, J. C. *Chem. Commun.* **2000**, 1197.
(16) Other MC₄M complexes for which more than one redox state has been characterized: Che, C.-M.; Chao, H.-Y.; Miskowski, V. M.; Li, Y.; Cheung, K.-K. *J. Am. Chem. Soc.* **2001**, *123*, 4985.
(17) Belanzoni, P.; Re, N.; Sgamellotti, A.; Floriani, C. *J. Chem. Soc., Dalton Trans.* **1998**, 1825.
(18) See also: (a) Belanzoni, P.; Re, N.; Rosi, M.; Sgamellotti, A.; Floriani, C. *Organometallics* **1996**, *15*, 4264. (b) Belanzoni, P.; Re, N.; Sgamellotti, A.; Floriani, C. *J. Chem. Soc., Dalton Trans.* **1997**, 4773. (c) Belanzoni, P.; Sgamellotti, A.; Re, N.; Floriani, C. *Inorg. Chem.* **2000**, *39*, 1147.
(19) Similar investigations of other carbon chain complexes: (a) Weyland, T.; Costuas, K.; Mari, A.; Halet, J.-F.; Lapinte, C. *Organometallics* **1998**, *17*, 5569. (b) Weyland, T.; Lapinte, C.; Frapper, G.; Calhorda, M. J.; Halet, J.-F.; Toupet, L. *Organometallic* **1997**, *16*, 2024. (c) Weyland, T.; Costuas, K.; Halet, J.-F.; Lapinte, C. *Organometallics* **2000**, *19*, 4228. (d) Koentjoro, O. F.; Rousseau, R.; Low, P. J. *Organometallics* **2001**, *20*, 4502.
(20) (a) Jiao, H.; Gladysz, J. A. *New. J. Chem.* **2001**, *25*, 551. (b) See also: Belanzoni, P.; Re, N.; Sgamellotti, A. *J. Organomet. Chem.* **2002**, *656*, 156.
(21) Coat, F.; Guillevic, M.-A.; Toupet, L.; Paul, F.; Lapinte, C. *Organometallics* **1997**, *16*, 5988.
(22) Denis, R.; Toupet, L.; Paul, F.; Lapinte, C. *Organometallics* **2000**, *19*, 4240.
(23) Roger, C.; Toupet, L.; Lapinte, C. *J. Chem. Soc., Chem. Commun.* **1988**, 713.

Table 1. Crystallographic Data for **1**·CH$_2$Cl$_2$ and **6**$^{3+}$ 3PF$_6^-$

	1·CH$_2$Cl$_2$	**6**$^{3+}$ 3PF$_6^-$
molecular formula	C$_{76}$H$_{78}$Fe$_2$P$_4$·CH$_2$Cl$_2$	2 × (C$_{26}$H$_{47}$F$_9$FeP$_{3.5}$)
molecular weight	1311.89	1389.76
crystal system	monoclinic	triclinic
space group	$P2_1/c$	P-1
cell dimensions		
a, Å	14.0040(10)	8.821(7)
b, Å	18.397(5)	10.743(2)
c, Å	25.243(6)	16.943(3)
α, deg	90.0	77.29(2)
β, deg	101.269(10)	89.44(3)
γ, deg	90.0	87.37(3)
V, Å^3	6473(2)	1564.6(13)
Z	4	2
d_{calc}, g/cm^3 (294 K)	1.346	1.475
absorption coeff (mm^{-1})	0.674	0.731
$F(000)$	2752	725
crystal dimensions (mm^3)	0.40 × 0.30 × 0.22	0.40 × 0.25 × 0.25
diffractometer	CAD4 NONIUS	CAD4 NONIUS
radiation (Å)	Mo Kα (0.709 26)	Mo Kα (0.710 69)
data collection method	$\omega/2\theta$	$\omega/2\theta$
t_{max}/measure, s	60	60
range/indices (h,k,l)	0, 17; 0, 23; −32, 32	0, 10; −12, 12; −20, 20
θ range	2.13 to 26.97	1.23 to 24.97
decay of standards (25), %	1.2	
reflections measured	14 598	5883
independent reflections	14 020	5490
obsd data, $I > 2\sigma(I)$	9309	4179
no. of variables	832	386
R_{int} (from mergin equiv reflns)	0.0169	0.0172
final R	0.0423 [$R_w = 0.0956$]	0.0728 [$R_w = 0.2198$]
R indices (all data)	0.0905 [$R_w = 0.1097$]	0.0927 [$R_w = 0.2336$]
GOF	1.006	1.069
largest diff peak and hole, eÅ^{-3}	0.3256 and −0.241	0.820 and −1.256

Table 2. Selected Distances (Å) and Angles (deg) for **1**·CH$_2$Cl$_2$ and **6**$^{3+}$ 3PF$_6^-$

1·CH$_2$Cl$_2$		**6**$^{3+}$ 3PF$_6^-$	
Fe1−P1	2.1687(10)	Fe1−P1	2.2775(16)
Fe1−P2	2.1692(8)	Fe1−P2	2.2581(19)
Fe2−P3	2.1634(8)		
Fe2−P4	2.1723(11)		
Fe1−C37	1.884(3)	Fe1−C25	1.804(5)
Fe2−C40	1.889(3)		
C37−C38	1.220(4)	C25−C26	1.231(7)
C38−C39	1.373(4)	C26−C26	1.342(9)
C39−C40	1.221(4)		
Fe1−Cp^a	1.738	Fe1−Cp^a	1.781
Fe2−Cp^a	1.737		
Fe1−Fe2	7.564	Fe1−Fe1	7.431
P1−Fe1−P2	85.70(3)	P1−Fe1−P2	85.31(6)
P1−Fe1−C37	84.60(9)	P1−Fe1−C25	85.45(16)
P2−Fe1−C37	81.92(8)	P2−Fe1−C25	88.21(16)
P3−Fe2−P4	86.20(3)		
P3−Fe2−C40	80.63(9)		
P4−Fe2−C40	82.50(9)		
Fe1−C37−C38	178.9(3)	Fe1−C25−C26	176.3(4)
Fe2−C40−C39	174.7(3)		
C37−C38−C39	176.8(3)	C25−C26−C26	178.5(7)
C38−C39−C40	177.0(3)		

^{a} Centroid of the η^5-C$_5$Me$_5$ ligand.
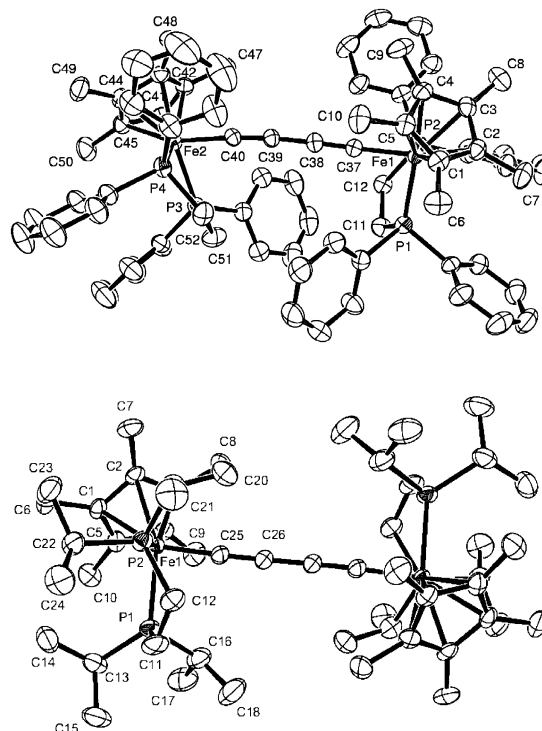
Figure 1. Structures of **1** (top) and the trication of **6**$^{3+}$ 3PF$_6^-$ (bottom) showing thermal ellipsoids at the 50% probability level.

accord with trends established for the mononuclear iron complexes [(η^5-C$_5$Me$_5$)(η^2-diphos)Fe(C≡CR)]$^{n+}$ nX$^-$ ($n = 0$, 1).[22] For example, the Fe−C$_\alpha$ bond is slightly shorter (1.830(9) Å), and this is analyzed together with other parameters in detail below. The Fe−Fe distance in **1** is slightly longer than that in **1**$^+$ PF$_6^-$ (7.564 vs 7.431 Å) and close to that of an unsymmetrical FeC$_4$Fe complex described previously (7.570 Å).[21] It is much shorter than that in the less electron-rich tetracarbonyl complex {(η^5-C$_5$Me$_5$)(CO)$_2$Fe}$_2$C$_4$ (7.653 Å) of Akita[24] and the Fe−Re and Re−Re distances in **3** and **2** (7.703 and 7.829 Å).[8]

Figure 1 also shows that the FeC$_4$Fe linkage in **1** deviates somewhat from linearity. However, the Fe−C$_\alpha$−C$_\beta$ angles

(178.8°, 174.6°) are less acute than those in **1**$^+$ PF$_6^-$ (167.0°).[9] This small deviation from linearity, likely due to packing effects, has been demonstrated in several related complexes.[25,26] The most salient difference between **1** and **1**$^+$ PF$_6^-$ would be the FeC$_4$Fe conformation. Here, it is convenient to define a twist angle (γ) using the centroid of the C$_5$Me$_5$ ligand on each endgroup, such that 180° and 0° correspond to *anti* and *syn*

(24) Akita, M.; Chung, M.-C.; Sakurai, A.; Sugimoto, S.; Terada, M.; Tanaka, M.; Moro-Oka, Y. *Organometallics* **1997**, *16*, 4882.

(25) Dembinski, R.; Lis, T.; Szafert, S.; Mayne, C. L.; Bartik, T.; Gladysz, J. A. *J. Organomet. Chem.* **1999**, *578*, 229.
(26) Mohr, W.; Stahl, J.; Hampel, F.; Gladysz, J. A. *Inorg. Chem.* **2001**, *40*, 3263.

arrangements. Accordingly, **1** exhibits an approximately orthogonal geometry ($\gamma = 78.9°$), while **1⁺** PF_6^- gives an *anti* arrangement ($\gamma = 180°$), a required consequence of the crystallographic inversion center. The crystal structures of **2** and **3** exhibit conformations closer to **1** ($\gamma = 107.6°$ and $48.3°$).[10]

As noted above, the replacement of the dppe ligands in the consanguineous family **1**ⁿ⁺ nPF_6^- by dippe ligands allows isolation of the trication **6**³⁺ 3PF_6^-.[11] The crystal structure was determined analogously to **1**. The result is shown in Figure 1 (bottom), and data are summarized in Tables 1 and 2. Compound **6**³⁺ 3PF_6^- is centrosymmetric, with an inversion center in the middle of the $C_\beta-C_{\beta'}$ bond. The asymmetric unit consists of one-half trication located on the 0.5, 0.5, 0.5 center of the symmetry, one PF_6^- anion in general positions and one-half PF_6^- anion on the 0, 0, 0.5 position. As a consequence, the iron endgroups are rigorously equivalent.

Crystalline **6**³⁺ 3PF_6^- exhibits a twist angle (γ) of 180°, like **1⁺** PF_6^- above. The Fe—P and Fe—C₅Me₅/centroid distances are significantly longer than those of **1** (2.2775(16)/2.2581(19) vs 2.1687(10)−2.1634(8)/2.1692(8)−2.1723(11) Å; 1.781 vs 1.738/1.737 Å) and correspond to typical iron(III) values in the (η^5-C₅R₅)(η^2-dppe)Fe series.[22] Within the C₄ chain, the Fe—C$_\alpha$ and $C_\beta-C_{\beta'}$ bonds are much shorter than those in **1** (1.804(5) vs 1.884(2)−1.889(2) Å; 1.342(9) vs 1.374(3) Å), as is the Fe—Fe distance (7.431 vs 7.564 Å). However, the $C_\alpha-C_\beta$ bond lengths do not differ within experimental error.

2. Preliminary Theoretical Analysis. Before presenting high-level DFT data, a qualitative analysis based upon extended Hückel theory (EHT) provides an instructive general perspective. Such analyses have been reported earlier for the model ruthenium complex **5**-**H**, using the frontier molecular orbitals (FMO) of the dianion C_4^{2-} and two cationic [(η^5-C₅H₅)(PH₃)₂- Ru]⁺ fragments.[14] Bonding is mainly governed by strong σ-type interactions between unoccupied high-lying metallic frontier orbitals and low-lying occupied C₄ orbitals, leading to an important electron donation from the C₄ spacer to the metal fragments. Additionally, significant metal−carbon π-type interactions occur but between occupied metal FMOs and occupied carbon orbitals rather than vacant carbon orbitals. Consequently, π-type back-donation is weak. Also, the closely spaced HOMO and HOMO-1 are metal−carbon antibonding, delocalized over the entire RuC₄Ru assembly and well separated from MOs strongly metal in character. It was concluded that any oxidation process should involve a loss of electrons from these MOs, considerably affecting both the metal centers and the carbon spacer, as experimentally observed.

These results should be transferable to the present systems **1**−**3**, since the rhenium and iron endgroups represent typical pseudo-ML₅ fragments with FMO patterns analogous to that of the ruthenium endgroup.[14] Indeed, EHT calculations on the model complexes {(η^5-C₅H₅)(η^2-H₂PCH₂CH₂PH₂)Fe}₂C₄ (**1**-**H**), {(η^5-C₅H₅)(NO)(PH₃)Re}₂C₄ (**2**-**H**), and (η^5-C₅H₅)(η^2-H₂PCH₂- CH₂PH₂)FeC₄Re(PH₃)(NO)(η^5-C₅H₅) (**3**-**H**), or the PH₃ analogues of **1**-**H** and **3**-**H**, yield similar conclusions, that is, weak π-type back donation and nearly degenerate π-type HOMO and HOMO-1 which result from four-electron repulsive interactions between metal and C₄ π FMOs and which are consequently M−C$_\alpha$ and $C_\beta-C_{\beta'}$ antibonding and $C_\alpha-C_\beta$ bonding and delocalized over the MC₄M moiety. A typical interaction diagram, that for the diiron species, is presented in Figure 2.
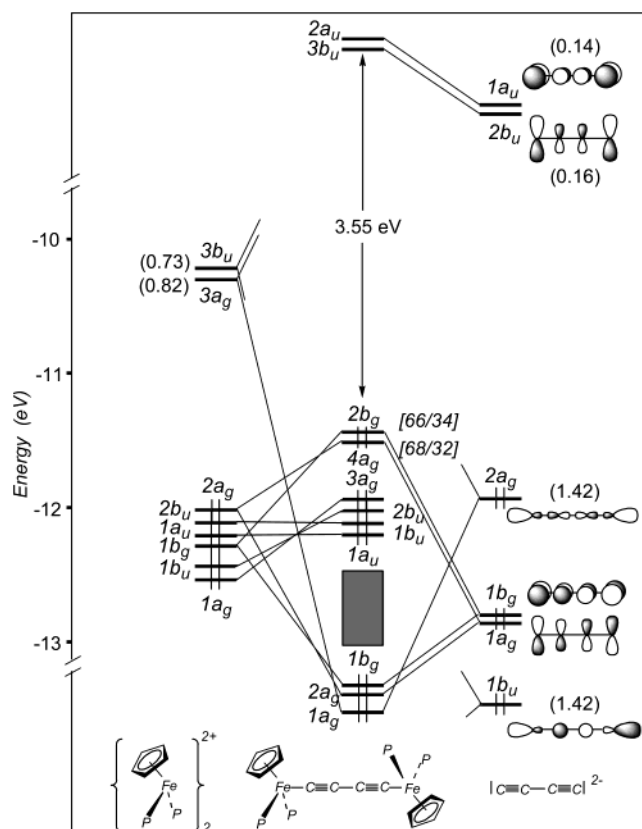

Figure 2. Extended Hückel orbital interaction diagram for the neutral model complex **1**-**H**.

This suggests that as oxidation proceeds, the M−C$_\alpha$ and $C_\beta-C_{\beta'}$ single bonds will shorten whereas the $C_\alpha-C_\beta$ triple bond will lengthen. However, to accurately address other important issues, such as bond orders and spin states, higher level computations are essential.

3. DFT Analysis; Diiron Complexes. DFT calculations using the Gaussian 98 and/or the ADF packages were performed on model compounds [**1**-**H**−**3**-**H**]ⁿ⁺ ($n = 0$−4) as described in the Experimental Section. Geometries were optimized for various oxidation and spin states, and results with the diiron series [**1**-**H**]ⁿ⁺ are presented first. Key data are given in Table 3, where **S**, **T**, **D**, and **Q** denote singlet, triplet, doublet, and quartet states, respectively. Good agreement is found between the bond lengths and angles computed for **1**-**H** and [**1**-**H**]⁺ and those of crystallographically characterized **1** and **1⁺** PF_6^- (also listed in Table 3). This enhances confidence in the structural parameters computed for compounds for which no X-ray data are available. Similar calculations were also conducted with {(η^5-C₅H₅)(CO)₂- Fe}₂C₄ as a model for the real complex {(η^5-C₅Me₅)(CO)₂- Fe}₂C₄. Again, agreement was excellent.[27]

To help clarify valence formulations, natural localized molecular orbital (NLMO) bond orders were computed and are summarized in Table 4. These clearly show that **1**-**H** is best described by an FeC≡CC≡CFe electronic structure. This is in accord with the structural data for **1** above, as well as the IR $\nu_{C≡C}$ values,[28] all of which fall into typical ranges. Complex **1**-**H** is C_i-symmetrical, leading to a twist angle γ of 180°, much

(27) Selected observed[24] and calculated (parentheses) structural parameters for {(CO)₂(η^5-C₅Me₅)Fe}₂C₄ (Å or deg): Fe−C$_\alpha$, 1.933 (1.913); C$_\alpha$−C$_\beta$, 1.197 (1.239); C$_\beta$−C$_{\beta'}$, 1.396 (1.378); Fe−C$_\alpha$−C$_{\beta'}$, 178.0 (179.2); C$_\alpha$−C$_\beta$−C$_{\beta'}$, 178.0 (178.6).
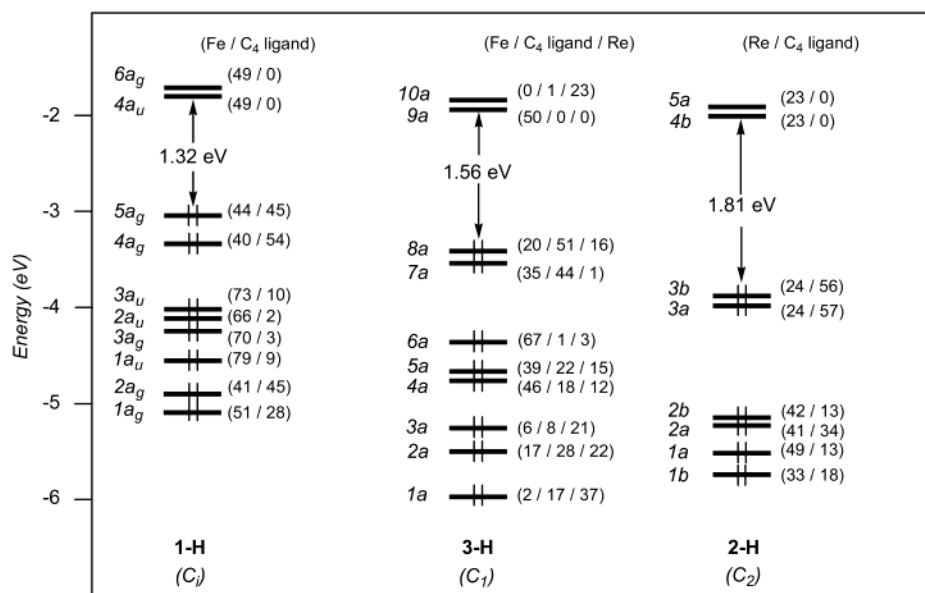
Figure 3. DFT molecular orbital diagrams of **1-H** (left), **2-H** (right), and **3-H** (middle) obtained using the ADF package. The metal/carbon chain percentage contributions of the MOs are given in brackets.

Table 3. Selected B3LYP Optimized Structural Parameters for Models $[1\text{-}H]^{n+}$ ($n = 0-4$) and Crystallographic Data for **1**, 1^+ PF_6^- and 6^{3+} $3PF_6^-$ (Å and deg)

parameter	1-H	1[c]	[1-H]+	1+ PF6− [d]	[1-H(S)]2+	[1-H(T)]2+	[1-H(D)]3+	[1-H(Q)]3+	63+ 3PF6− [c]	[1-H]4+
Fe−Cα	1.917	1.884−1.889	1.832	1.829	1.764	1.759	1.703	1.852	1.804	1.648
Cα−Cβ	1.248	1.220	1.264	1.238	1.287	1.288	1.320	1.268	1.231	1.367
Cβ−Cβ′	1.382	1.374	1.349	1.357	1.319	1.317	1.288	1.344	1.342	1.258
Fe−P[a]	2.221	2.1687	2.240	2.222	2.262	2.268	2.291	2.328	2.2775−2.2581	2.324
Fe−Cp[b]	1.759	1.738−1.737	1.757	1.767	1.763	1.772	1.780	1.787	1.781	1.800
Fe−Fe	7.705	7.564	7.542	7.431	7.418	7.443	7.323	7.578	7.431	7.276
Fe−Cα−Cβ	175.5	178.8−174.6	178.9	167.0	177.1	176.4	174.4	175.3	176.3	173.5
Cα−Cβ−Cβ′	178.7	176.8−175.5	178.5	177.3	178.9	179.7	179.8	179.6	178.5	179.2
P−Fe−Cα[a]	83.3	86.8	87.7	89.0	92.0	92.3	96.0	94.0	88.21−85.31	99.7
Cp−Fe−Fe−Cp (γ)	180.0	78.9	180.0	180.0	180.0	180.0	180.0	180.0	180.0	180.0

[a] Averaged. [b] Centroid of the η^5-C_5R_5 ligand. [c] This work. [d] Reference 9.

Table 4. B3LYP Calculated NLMO Bond Orders for $[1\text{-}H]^{n+}$

complex	Fe−Cα	Cα−Cβ	Cβ−Cβ′	Fe−P[a]
1-H	0.579	2.621	1.141	0.506
[1-H]+	0.789	2.397	1.394	0.538
[1-H(S)]2+	0.925	1.994	1.840	0.565
[1-H(T)]2+	1.020	1.973	1.824	0.569
[1-H(D)]3+	1.182	1.708	2.077	0.638
[1-H(Q)]3+	0.722	2.347	1.455	0.549
[1-H]4+	1.234	1.270	2.592	0.711

[a] Averaged.

larger than the 78.9° observed. This is believed to have a simple steric and/or electronic explanation: in the real molecules, as opposed to the model compounds, weak $\pi-\pi$ interactions between phenyl rings may occur stabilizing the observed conformation. Indeed, calculations on the model compounds

(28) (a) Experimental IR $\nu_{C\equiv C}$ or $\nu_{C=C=C}$ values (cm^{-1}, CH_2Cl_2): **1**, 1955(vs); 1^+ PF_6^-, 1973(s), 1880(m); 1^{2+} $2PF_6^-$, 1950(vs), 2160(w); 6^{3+} $3PF_6^-$, none observed; **2**, 1964(w) (Raman, 2056(s)); 2^+ PF_6^-, 1872(m) (Raman, 1990-(s)); 2^{2+} $2PF_6^-$, none observed (Raman, 1883(s)); **3**, 2095(sh), 2058(m), 1956(m); 3^+ PF_6^-, 2055(sh), 1950(vs), 1882(m); 3^{2+} $2PF_6^-$, 1949(w), 1851-(vw), 1787(w). (b) Calculated IR-active $\nu_{C\equiv C}$ or $\nu_{C=C=C}$ values (cm^{-1}): **1-H**, 1962; **[1-H]+**, 1879; **[1-H(S)]2+**, 1771; **[1-H(T)]2+**, 1535; **[1-H(D)]3+**, 1626; **[1-H(Q)]3+**, 1783; **[1-H]4+**, 1461; **2-H**, 1966, 2075; **[2-H]+**, 1872; **[2-H(S)]2+**, 1768, 1974; **[2-H(T)]2+**, 1756, 1794; **3-H**, 1965, 2095; **[3-H]+**, 1881, 2012; **[3-H(S)]2+**, 1768, 1970; **[3-H(T)]2+**, 1881, 1823 (CC/NO), 1825 (CC/NO). The calculated vibrational frequencies were scaled by an empirical factor of 0.9667. See Huo, C.-F.; Li, Y.-W.; Wu, G.-S.; Beller, M.; Jiao, H. *J. Phys. Chem. A* **2002**, *106*, 12161.

show a very flat potential energy surface with respect to the orientation of the metal fragments.

The molecular orbital diagram of **1-H** obtained with the ADF package is shown on the left-hand side of Figure 3. It is qualitatively similar to the EHMO diagram given in Figure 2, with a rather large energy gap separating the occupied and vacant orbital sets (1.32 eV). The delocalized nature of the HOMO and HOMO-1 over the MC$_4$M moiety deduced from the preliminary qualitative theoretical analysis is confirmed by DFT computations. The HOMO (5a$_g$) is 44% metal and 45% C$_4$ in character, and the HOMO-1 (4a$_g$) contains 40% metal and 54% C$_4$ character. Clearly, oxidation should affect bonding over the entire FeC$_4$Fe linkage. Indeed, upon going from **1-H** to the radical cation **[1-H]+**, the Fe−C$_\alpha$ and C$_\beta$−C$_{\beta'}$ bonds shorten and the C$_\alpha$−C$_\beta$ bond elongates (Table 3). This is in accord with the X-ray data for **1** and 1^+ PF_6^-. For example, the C$_\alpha$−C$_\beta$ bond length increases by 0.018 Å in the real systems, as opposed to 0.016 Å in the model compounds. The NMLO bond orders exhibit analogous patterns (Table 4).

At first glance, the IR data for 1^+ PF_6^- might appear contradictory, as the $\nu_{C\equiv C}$ values remain essentially constant.[28] Indeed, upon oxidation of similar mononuclear iron alkynyl complexes, the $\nu_{C\equiv C}$ values decrease by ca. 90 cm^{-1} without significant decrease in C≡C bond length.[22] On the other hand, the butatrienylidene complex $[(\eta^5$-$C_5Me_5)(\eta^2$-dppe)Fe=

Table 5. B3LYP Computed Mulliken Total Atomic Spin Densities for the Open-Shell Systems $[1\text{-H}]^{n+}$, $[2\text{-H}]^{n+}$, and $[3\text{-H}]^{n+}$

complex	M	C_α	C_β	NO
$[1\text{-H}]^+$	0.336/Fe	0.123/C_α	0.083/C_β	
$[2\text{-H}]^+$	0.252/Re	0.158/C_α	0.106/C_β	
$[3\text{-H}]^+$	0.194/Re	0.147/C_α	0.075/C_β	
	0.447/Fe	0.108/$C_{\alpha'}$	0.107/$C_{\beta'}$	
$[1\text{-H(T)}]^{2+}$	0.658/Fe	0.258/C_α	0.169/C_β	
$[2\text{-H(T)}]^{2+}$	0.366/Re	0.276/C_α	0.186/C_β	0.128/NO
$[3\text{-H(T)}]^{2+}$	0.446/Re	0.138/C_α	0.218/C_β	
	1.034/Fe	0.161/$C_{\alpha'}$	0.118/$C_{\beta'}$	
$[1\text{-H(D)}]^{3+}$	0.216/Fe	0.204/C_α	0.097/C_β	
$[1\text{-H(Q)}]^{3+}$	1.363/Fe	0.190/C_α	0.191/C_β	

$C=C=C=C(H)Fe(CO)_2(\eta^5\text{-}C_5Me_5)]^+$ OTf⁻ exhibits an IR band at 1952 cm⁻¹,[29] whereas $(\eta^5\text{-}C_5Me_5)(\eta^2\text{-dppe})FeC_4Fe(CO)_2(\eta^5\text{-}C_5Me_5)$ gives an absorption at 2109 cm⁻¹.[21] Interestingly, a decrease of 83 cm⁻¹ is computed for the $\nu_{C\equiv C}$ upon going from **1-H** to $[1\text{-H}]^+$ in agreement with the calculated $C_\alpha-C_\beta$ bond lengthening.[28] Clearly, some care must be taken in assigning cumulenic or acetylenic forms to such complexes based upon IR data alone.

To probe the delocalization of the odd electron of $[1\text{-H}]^+$, atomic spin densities were calculated, as summarized in Table 5. In accord with an extensively delocalized system, 67% of the single electron is located at the two iron centers (0.336/Fe), with the remaining 33% distributed over the C_4 chain. The spin density at iron is strongly supported by the Mössbauer quadrupole splitting (QS) of 1^+ PF_6^-, which is the average of the characteristic QS values of Fe(II) and Fe(III) centers in the $(\eta^5\text{-}C_5Me_5)Fe(\eta^2\text{-dppe})$ series.[9] Additional evidence for the "class III" nature of this mixed valence compound has been fully treated in earlier papers. Taken together, the above experimental and computational data clearly indicate that the electronic structure is a hybrid of all resonance structures given for **Ib** in Scheme 4 but with dominant $^{1/2(+\bullet)}FeC\equiv CC\equiv CFe^{1/2(+\bullet)}$ character.

Attention was next turned to the structure and spin states of the dication $[1\text{-H}]^{2+}$. The energy computed for the singlet $[1\text{-H(S)}]^{2+}$ was 1.9 kcal/mol higher than that of the triplet $[1\text{-H(T)}]^{2+}$, a value that is within the limit of accuracy of the method and suggests the states are isoenergetic. DFT calculations with the ADF package led to the same conclusion. Additional calculations using the broken-symmetry formalism (Experimental section) did not show any asymmetry of the optimized geometry of $[1\text{-H(S)}]^{2+}$. In contrast, the singlet diruthenium complex $[5\text{-H(S)}]^{2+}$ is computed to be 2.3 kcal/mol lower in energy than $[5\text{-H(T)}]^{2+}$.[14] With 5^{2+} $2PF_6^-$, all experimental data is consistent with the cumulenic electronic structure $^+Ru=C=C=C=C=Ru^+$.[14] The potential energy surface for rotating the endgroups in $[1\text{-H(S)}]^{2+}$ is quite flat, and conformations with other γ values are close in energy.

Importantly, magnetic susceptibility, IR, and Mössbauer data for the diiron complex 1^{2+} $2PF_6^-$ are best modeled by a high-spin/low-spin triplet/singlet equilibrium.[9,11,12] For example, magnetic susceptibility measurements indicate dominant antiferromagnetic character at low temperature but evidence some paramagnetic character as the temperature rises.[9] Indeed, the singlet ground state (**S**) is very weakly separated from the triplet

state (**T**) ($J = -18$ cm⁻¹ or 0.05 kcal/mol). Both states are statistically populated ((**S**)/(**T**) 25:75), even at liquid nitrogen temperature.[12] Interestingly, the IR $\nu_{C\equiv C}$ values are greater than those of **1** and 1^+ PF_6^-.[28]

No crystallographic data for this oxidation state are yet available. However, Table 3 shows that $[1\text{-H(S)}]^{2+}$ and $[1\text{-H(T)}]^{2+}$ have very similar bond lengths. As compared to **1-H** or $[1\text{-H}]^+$, there is a continued contraction of the $Fe-C_\alpha$ bond (1.917 to 1.832 to 1.764–1.759 Å) and $C_\beta-C_{\beta'}$ bond (1.382 to 1.349 to 1.319–1.317 Å), and a simultaneous elongation of the $C_\alpha-C_\beta$ bond (1.248 to 1.264 to 1.287–1.288 Å). As illustrated in Table 4, the NMLO bond orders of $[1\text{-H(S)}]^{2+}$ and $[1\text{-H(T)}]^{2+}$ are also similar. Analogous patterns are found with **5-H**, $[5\text{-H}]^+$, $[5\text{-H(S)}]^{2+}$, $[5\text{-H(T)}]^{2+}$,[14] and related compounds below. With reference to Figure 3, a double oxidation of the HOMO (singlet product) or two single oxidations of the HOMO and HOMO-1 (triplet product) have nearly the same net affect on bonding interactions. In this light, it is not so surprising that the bond lengths computed for $[1\text{-H(S)}]^{2+}$ and $[1\text{-H(T)}]^{2+}$ are so similar.

The atomic spin densities calculated for $[1\text{-H(T)}]^{2+}$ (Table 5) show another highly delocalized system, with 1.316 of the two unpaired electrons located on the two iron centers (66%). To rationalize the spin density on carbon, resonance forms of the types shown for **Ic**-(**T**) in Scheme 4 must be invoked. However, the data suggest a dominant $^{\bullet+}FeC\equiv CC\equiv CFe^{+\bullet}$ electronic structure.

Attention was next turned to the trication $[1\text{-H}]^{3+}$ and another question of spin state. From an EHT perspective, a doublet state would correspond to the removal of three electrons from the HOMO or HOMO-1 in Figure 2. Surprisingly, the doublet $[1\text{-H(D)}]^{3+}$ was found to be 8.4 kcal/mol *less* stable than the quartet $[1\text{-H(Q)}]^{3+}$ using the Gaussian package at the B3LYP hybrid density functional level of theory. The latter must have three unpaired electrons, and in the context of Figure 3, this would imply single occupation HOMO, HOMO-1, and HOMO-2. The last has much more metal character (73%) than the first two (40–44%). Because of the different makeup of these MOs, the bond lengths computed for $[1\text{-H(D)}]^{3+}$ and $[1\text{-H(Q)}]^{3+}$ differ substantially (Table 3).

The crystallographic bond lengths of 6^{3+} $3PF_6^-$ (Table 2) fit slightly better with those computed for the quartet $[1\text{-H(Q)}]^{3+}$ (Table 3). Nevertheless, the deviations are larger than with **1** and 1^+ PF_6^-. In particular, the computed $Fe-C_\alpha$ distance is 0.048 Å too long. Conversely, the doublet $[1\text{-H(D)}]^{3+}$ exhibits an $Fe-C_\alpha$ distance 0.101 Å too short. Since 6^{3+} $3PF_6^-$ seems a rough average of the two computed structures, there is the possibility that it exists as a mixture of spin states at room temperature. Magnetic susceptibility measurements indicate a ground state doublet ($J = -100$ cm⁻¹) but that a spin transition takes place with the excited quartet state in the 4–290 K range.[30] Interestingly, ADF computations using the BP86 functional indicate that $[1\text{-H(D)}]^{3+}$ is energetically *favored* by 8.3 kcal/mol, in agreement with experiment. We do not understand the origin of the discrepancy between the B3LYP results and experimental magnetic data.

(29) Coat, F.; Guillemot, M.; Paul, F.; Lapinte, C. *J. Organomet. Chem.* **1999**, *578*, 76.

(30) (a) Guillemot, M. Ph.D. Thesis, Université de Rennes 1, 1998. (b) Guillemot, M.; Lapinte, C. Unpublished results.

Table 6. Selected B3LYP Optimized Structural Parameters for Models [2-H]$^{n+}$ (n = 0−2) and Crystallographic Data for **2** and **2**$^{2+}$ 2PF$_6^-$ (Å and deg)

parameter	[2-H]	2^a	[2-H]$^{+ b}$	[2-H(S)]$^{2+ b}$	2^{2+} 2PF$_6^{- a}$	[2-H(T)]$^{2+}$
Re−C$_\alpha$	2.024	2.037	1.964/1.964	1.906/1.907	1.909−1.916	1.929
C$_\alpha$−C$_\beta$	1.247	1.202	1.265/1.265	1.290/1.290	1.263−1.260	1.284
C$_\beta$−C$_{\beta'}$	1.371	1.389	1.339/1.339	1.307/1.308	1.305	1.318
Re−P	2.379	2.375	2.401/2.402	2.439/2.438	2.439−2.430	2.441
Re−N	1.768	1.754	1.783/1.783	1.791/1.790	1.777−1.767	1.798
Re−Cp^c	1.993	1.964	2.001/2.001	2.012/2.012	1.972−1.963	2.004
N−O	1.192	1.190	1.178/1.178	1.167/1.167	1.179−1.184	1.166
Re−Re	7.909	7.828	7.795/7.795	7.692/7.692	7.635	7.738
Re−C$_\alpha$−C$_\beta$	176.6	174.4	176.4/178.5	174.8/176.1	168.5−171.4	176.4
C$_\alpha$−C$_\beta$−C$_{\beta'}$	178.1	176.8	178.2/179.1	178.9/178.1	177.8−175.4	179.4
N−Re−C$_\alpha$	98.9	100.7	97.0/96.9	96.9/96.6	103.2−101.7	96.2
P−Re−C$_\alpha$	80.5	82.4	86.8/86.2	93.7/92.9	88.6−92.4	91.0
P−Re−N	92.9	92.8	92.6/92.5	92.0/91.7	93.7−87.7	93.0
Re−N−O	176.8	170.9	175.7/175.8	175.2/175.5	167.8−171.7	175.1
Cp−Re−Re−Cp (γ)	155.9	107.6	130.7/41.4	120.7/53.7	117.1	33.5
P−Re−Re−P	94.3	153.9	26.5/149.5	18.4/158.6	18.4	73.7
N−Re−Re−N	83.2	25.3	147.8/34.7	155.5/25.4	155.5	113.3

^{a} Reference 8. ^{b} For syn/anti isomers; see Figure 4. ^{c} Centroid of the η^5-C$_5$R$_5$ ligand.

How are the electronic structures of these trication systems best described? Scheme 4 depicts some of the plethora of resonance forms possible for the doublet (**Id**-(**D**)) and quartet (**Id**-(**Q**)). The crystal structure of **6**$^{3+}$ 3PF$_6^-$ together with certain electronic transitions suggest that the backbone exhibits some cumulenic character.[5f,11] This is supported by the NMLO bond orders computed for the doublet [**1-H(D)**]$^{3+}$ (Table 4), which compare rather well with those of the cumulenic dication [**1-H(S)**]$^{2+}$. The bond orders computed for the quartet [**1-H(Q)**]$^{3+}$ compare quite well with those for the cation radical [**1-H**]$^+$.

Experimental results also suggest that compound **6**$^{3+}$ 3PF$_6^-$ is a class III mixed valence species,[11,5b] consistent with the computational data for both spin states. For [**1-H(D)**]$^{3+}$, the one unpaired electron is ca. 60% delocalized on the carbon bridge (Table 5). This suggests that slightly greater weight should be given to the bottom four resonance forms in Scheme 4, which also delocalize positive charge onto the bridge. For [**1-H(Q)**]$^{3+}$, the three unpaired electrons are ca. 78% delocalized on iron. However, this leaves ca. 65% of a single electron on the bridge. The valence-delocalized structure of [**1-H(D)**]$^{3+}$ is supported by additional calculations using the broken-symmetry formalism (Experimental Section), which did not show any asymmetry of its optimized geometry.

Finally, attention was turned to the tetracation [**1-H**]$^{4+}$, real analogues of which are experimentally inaccessible. As summarized in Table 3, the computed Fe−C$_\alpha$ and C$_\beta$−C$_{\beta'}$ bonds are much shorter than in any of the previous compounds (1.648 and 1.258 Å), and the C$_\alpha$−C$_\beta$ bond much longer (1.367 Å). The corresponding NMLO bond orders are also substantially higher and lower (Table 4). Thus, it can be concluded that [**1-H**]$^{4+}$ is best modeled by a bis(carbyne) or $^{2+}$Fe≡CC≡CC≡Fe^{2+} electronic structure (**Ic**, Scheme 2). Analogous results were obtained for the diruthenium tetracation **5**$^{4+}$ 4PF$_6^-$ and [**5-H**]$^{4+}$, the former of which could be characterized by IR.[14]

4. DFT Analysis; Dirhenium Complexes. The dirhenium model compounds [**2-H**]$^{n+}$ (n = 0−2) were studied next. In contrast to [**1-H**]$^{n+}$, the endgroups are chiral. Only the *rac* diastereomer series, two members of which have been crystallographically characterized,[8] was investigated. Importantly, the replacement of an iron phosphine ligand by a better π-accepting

rhenium nitrosyl ligand renders the endgroup less electron-rich, as further analyzed below. Key structural data are summarized in Table 6.

The bond lengths in **2-H**, which is of C_2 symmetry, generally fall into the range found for **2** crystallographically. The C$_\alpha$−C$_\beta$ bond shows the greatest deviation, 0.045 Å longer than observed.[8] The relative conformations of the endgroups are illustrated in Figure 4 (top). These differ from the experimental system, as reflected by the angle γ (155.9° vs 107.6°) or the P−Re−Re−P torsion angles (94.3° vs 153.9°). However, the potential energy surface for rotation is relatively flat. The metrical parameters, together with the NLMO bond orders in Table 7, clearly indicate a ReC≡CC≡CRe electronic structure. The C−C bond orders are essentially identical to those of the diiron analogue **1-H**. However, the M−C$_\alpha$ bond order is higher (0.746 vs 0.579), consistent with diminished repulsive and/or enhanced attractive bonding interactions.

The energy level scheme associated with **2-H** is quite similar to that of **1-H**, with the HOMOs 3a and 3b nearly degenerate and separated from both the high-lying LUMOs by 1.81 eV and, to a lesser extent, from the low-lying metal-based occupied MOs (see the right-hand side of Figure 3). Nevertheless, a shift to lower energy is noted for these HOMOs which are less heavily weighted on the metal atoms than in the corresponding MOs of **1-H** (ca. 25% vs ca. 40%).

The dirhenium dication was modeled next. As in the diiron series, both a singlet [**2-H(S)**]$^{2+}$ and a triplet [**2-H(T)**]$^{2+}$ were considered. As shown in Figure 4, two minima were found for the former, differing in the relative orientations of the endgroups. The PH$_3$ ligands are roughly *syn* in one and *anti* in the other (P−Re−Re−P torsion angles 18.4° and 158.6°). The bond lengths and angles are very close and listed side-by-side in Table 6. The former was slightly more stable (0.13 kcal/mol). These conformations can easily be rationalized as described previously[8] from FMO theory and the well-established rhenium fragment highest occupied FMO depicted in Figure 4. They are analogous to geometric isomers about a butatriene of formula ABC=C= C=CAB.

Complex **2**$^{2+}$ 2PF$_6^-$ crystallizes with the two bulky PPh$_3$ ligands in a contrasteric *syn* orientation, with a P−Re−Re−P torsion angle of 18.4°, exactly as found computationally. A
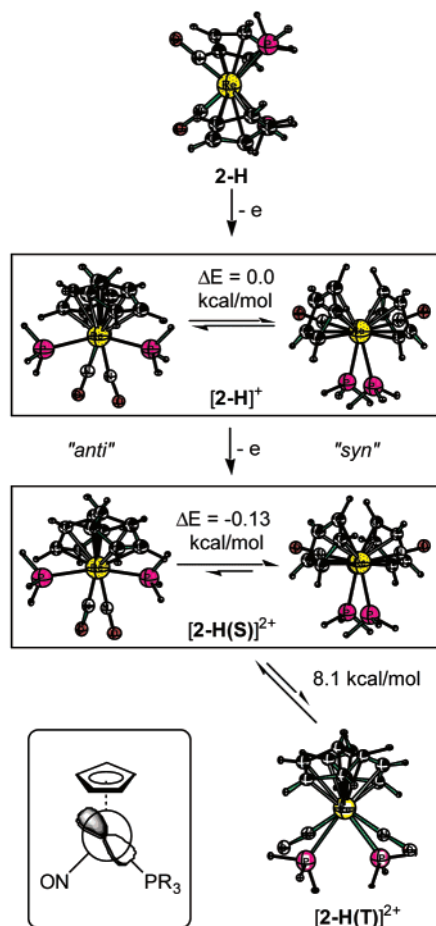
Figure 4. Computed structures of dirhenium complexes [**2**-**H**]ⁿ⁺. The highest occupied FMO of the $[(\eta^5\text{-}C_5H_5)(NO)(PR_3)Re]^+$ fragment is illustrated on the bottom left.

Table 7. B3LYP Calculated NLMO Bond Orders for [**2**-**H**]ⁿ⁺

complex	Re–C_α	C_α–C_β	C_β–$C_{\beta'}$	Re–P	N–O
2-H	0.746	2.618	1.167	0.598	1.300
[**2-H**]⁺	0.882	2.290	1.501	0.598	1.360
[**2-H(S)**]²⁺	1.280	1.965	1.861	0.647	1.440
[**2-H(T)**]²⁺	1.087	2.027	1.598	0.604	1.441

second isomer can be detected in solution by NMR. The equilibrium constant is 38:62 in CD_2Cl_2 at −93 °C, and the interconversion barrier, ca. 12 kcal/mol.[8] As shown in Table 6, the calculated and observed bond lengths and angles are in good agreement. The greatest deviation is again in the C_α–C_β bond, which is 0.027–0.030 Å longer than found. As with the diiron compounds, the M–C_α bond is shorter than in the neutral analogue (1.906–1.916 Å vs 2.024–2.037 Å).

The triplet [**2-H(T)**]²⁺ was computed to be 8.1 kcal/mol less stable than the singlet [**2-H(S)**]²⁺. Indeed, DFT calculations indicate that the dirhenium dication [**2-H(S)**]²⁺ exhibits a much larger HOMO/LUMO energy gap than the diiron dication [**1-H-(S)**]²⁺ (0.78 vs 0.17 eV, respectively). Such an energy gap favors the singlet state. Consequently, it is not surprising that the energy difference between the singlet and the triplet state is much larger for the former.

As in the diiron series, the bond lengths are quite close (Table 6). The C_α–C_β and C_β–$C_{\beta'}$ bonds showed a slightly greater degree of alternation (1.284 and 1.318 Å vs 1.290 and 1.307 Å), and the Re–Re distance increased (7.738 vs 7.692 Å). As

illustrated in Figure 4, the endgroup conformations are distinctly different, with a P–Re–Re–P torsion angle of 73.7° in the triplet. In this context, it deserves emphasis that the 8.1 kcal/mol energy gap is for the most favorable conformation of each spin state. As is well-known from potential energy surfaces of alkenes, the energy difference for a singlet and triplet state of identical conformation can be much less. Thus, the endgroup conformations in [**2-H**]²⁺ have a much greater influence on structural and electronic properties than in **2-H**.

The NLMO bond orders summarized for [**2-H(S)**]²⁺ and [**2-H(T)**]²⁺ in Table 7 show roughly the same pattern as the diiron complexes [**1-H(S)**]²⁺ and [**1-H(T)**]²⁺ in Table 4. In both cases, the singlets exhibit the greater M–C_α and C_β–$C_{\beta'}$ bond orders, and the triplets the greater C_α–C_β bond order. This is consistent with dominant $^+M{=}C{=}C{=}C{=}C{=}M^+$ and $^{\bullet+}MC{\equiv}CC{\equiv}CM^{+\bullet}$ electronic structures as proposed above. However, as noted for **2-H** and **1-H**, the rhenium compounds always exhibit greater M–C_α bond orders (1.280 vs 0.925 and 1.087 vs 1.000). Also, Table 5 shows that the spin density in [**1-H(T)**]²⁺ is less concentrated on rhenium, largely due to the acceptor properties of the nitrosyl ligand. Importantly, the NMR, IR, Raman, and magnetic properties of **2**²⁺ 2PF₆⁻ unambiguously show it to be a ground state singlet, with no low-lying thermally accessible triplet.[8]

In contrast to **2** and **2**²⁺ 2PF₆⁻, neither experimental nor computed model structures are available for the cation radical **2**⁺ PF₆⁻. IR and Raman data suggest ReC₄Re bond orders intermediate between those of **2** and **2**²⁺ 2PF₆⁻.[28] This is confirmed by the results with [**2-H**]⁺, which show C–C stretching frequencies,[28] bond lengths, and orders intermediate between those of **2-H** and [**2-H**]²⁺ (Tables 6 and 7). However, as illustrated in Figure 4, two endgroup conformations of equal energy are found. They are very similar to the *syn/anti* isomers of [**2-H(S)**]²⁺, with slight distortions in directions that would relieve nonbonding interactions (P–Re–Re–P torsion angles 26.5° vs 18.4° and 149.5° vs 158.6°). This indicates incipient multiple bonding for the Re–C_α and C_β–$C_{\beta'}$ linkages.

As shown in Table 5, the unpaired electron of [**2-H**]⁺ is delocalized over the ReC₄Re assembly. For both isomers, nearly half of the spin density is found on the rhenium atoms, and the rest, on the carbon chain. Note that, with the diiron analogue [**1-H**]⁺, about ²⁄₃ of the spin density is found on the metal atoms. This is further evidence for a greater degree of M–C_α multiple bonding in the dirhenium compound. In any event, the computational data are fully consistent with the earlier assignment **2**⁺ PF₆⁻ as a class III mixed valence compound based upon IR and ESR data.

Returning to Scheme 4, the oxidation chemistry of Berke's dimanganese complex **4** is highly relevant to the above data.[13] As noted above, each manganese moiety in the uncharged parent molecule carries 17 valence electrons. This gives a triplet ground state, which Berke has shown experimentally and computationally to be best modeled by the electronic structure $^{\bullet}MnC{\equiv}CC{\equiv}CMn^{\bullet}$. In principle, a singlet with $Mn{=}C{=}C{=}C{=}C{=}Mn$ character should also be possible. However, like the interaction diagram in Figure 2, the HOMO and HOMO-1 energies of this system are also very close, and singly occupied orbitals are energetically more favorable. Note that the symmetries of **1** and **4** are higher than the dirhenium complex **2**, and that the carbon chains are flanked by poor π-accepting *cis* ligands. Interestingly,

Table 8. Selected B3LYP Optimized Structural Parameters (Å and deg) for Models [**3-H**]$^{n+}$ ($n = 0-2$) and Crystallographic Data for **3**

parameter	3-H	3[a]	[3-H]$^+$	[3-H(S)]$^{2+}$	[3-H(T)]$^{2+}$
Re$-$C$_\alpha$	2.032	2.029	1.974	1.911	1.948
C$_\alpha$$-C_\beta$	1.246	1.224	1.262	1.288	1.270
C$_\beta$$-C_{\beta'}$	1.376	1.370	1.345	1.313	1.340
Fe$-$C$_{\alpha'}$	1.909	1.895	1.823	1.754	1.838
C$_{\alpha'}$$-C_{\beta'}$	1.249	1.209	1.265	1.290	1.265
Re$-$P	2.380	2.353	2.393	2.434	2.434
Re$-$N	1.769	1.752	1.781	1.789	1.791
N$-$O	1.193	1.212	1.180	1.168	1.168
Fe$-$P$'^b$	2.224	2.175	2.245	2.263	2.295
Re$-$Cp^c	1.989	1.965	2.001	2.011	2.003
Fe$-$Cp$'^c$	1.748	1.749	1.759	1.763	1.774
Re$-$Fe	7.805	7.730	7.654	7.530	7.629
Re$-$C$_\alpha$$-C_\beta$	176.0	169.6	178.1	175.5	174.8
C$_\alpha$$-C_\beta$$-C_{\beta'}$	177.8	177.4	178.1	178.6	177.7
Fe$-$C$_{\alpha'}$$-C_{\beta'}$	175.3	176.6	177.4	175.6	175.3
C$_{\alpha'}$$-C_{\beta'}$$-C_\beta$	179.1	178.3	176.7	176.1	177.4
P$-$Re$-$C$_\alpha$	78.8	83.0	86.4	93.0	91.2
P$-$Fe$-$C$_{\alpha'}$	83.6	84.8	88.6	92.7	91.1
N$-$Re$-$C$_\alpha$	99.1	103.4	97.0	96.9	95.9
P$-$Re$-$N	93.1	93.6	92.6	91.5	92.3
Re$-$N$-$O	176.5	171.8	175.4	175.6	175.5
Cp$-$Re$-$Fe$-$Cp$'$ (γ)	108.2	47.9	151.3	149.4	61.6

[a] Reference 10. [b] Averaged. [c] Centroid of the η^5-C$_5$R$_5$ ligand.

Table 9. B3LYP Calculated NLMO Bond Orders for [**3-H**]$^{n+}$

bond	3-H	[3-H]$^+$	[3-H(S)]$^{2+}$	[3-H(T)]$^{2+}$
Re$-$C$_\alpha$	0.744	0.818	1.265	1.013
C$_\alpha$$-C_\beta$	2.654	2.385	2.020	2.184
C$_\beta$$-C_{\beta'}$	1.154	1.371	1.839	1.390
C$_{\alpha'}$$-C_{\beta'}$	2.585	2.334	1.927	2.324
Fe$-$C$_{\alpha'}$	0.582	0.854	1.045	0.728
Re$-$P	0.599	0.604	0.647	0.592
N$-$O	1.294	1.352	1.435	1.412
Fe$-$P^a	0.506	0.538	0.545	0.555

[a] Averaged.

the ground state of the oxidation product, **4**$^+$ PF$_6$$^-$, is a doublet as opposed to a quartet. Further oxidation gives the dication **4**$^{2+}$ 2PF$_6$$^-$, which is a singlet. All compounds in this series have been structurally characterized.

5. DFT Analysis; Rhenium/Iron Complexes. The heterobimetallic model complexes [**3-H**]$^{n+}$ ($n = 0-2$) were studied next. Their unsymmetrical nature introduces the possibility of polarized electronic structures. In this series, only **3** (Figure 1) has been crystallographically characterized.[10] As summarized in Table 8, the bond lengths and angles computed for **3**-**H** compare satisfactorily with those found for **3**. However, as observed with **2**-**H**, the computed and observed twist angles γ differ slightly (108.2° vs 132.1°). The NLMO bond orders are summarized in Table 9. The values for the Re$-$C$_\alpha$$-C_\beta$ linkages are similar to those in **2**-**H**, and the values for the Fe$-$C$_{\alpha'}$$-C_{\beta'}$ linkages are very similar to those in **1**-**H**. Accordingly, the ReC$_4$-Fe moiety is slightly polarized but well described by an ReC≡CC≡CFe valence formulation. Systems with strongly donating and accepting metal fragments could, for example, give rise to electronic structures best represented by $^+$M=C=C=C=C=M$^-$.

The structural parameters found for cation radical [**3-H**]$^+$ (Table 8) are close to those of [**1-H**]$^+$ and [**2-H**]$^+$ (Tables 3, 6). In particular, the bond lengths of the Re$-$C$_\alpha$$-C_\beta$ linkages are similar to those in **2**-**H**, and those for the Fe$-$C$_{\alpha'}$$-C_{\beta'}$ linkages are similar to those in **1**-**H**. However, the NMLO bond order data (Table 9) show a higher Fe$-$C$_{\alpha'}$ value than in **1**-**H** (0.854 vs 0.789) and a lower Re$-$C$_\alpha$ value than in **2**-**H** (0.818

vs 0.882). This, coupled with similar but less pronounced trends in the bond lengths, suggests enhanced M$-$C$_\alpha$ multiple bond character for the iron terminus.

The calculated atomic spin densities in Table 5 unequivocally establish a strongly polarized structure. The electron density on iron is more than twice that on rhenium (0.447 vs 0.194). This was expected from the DFT molecular orbital diagram of the neutral complex **3**-**H** which shows a very poor contribution of the rhenium atom in the two HOMOs (16 and 1%, see the middle of Figure 3) which are depopulated upon oxidation. This is consistent with the more electron-releasing character of the iron fragment (vide infra), which would favor an electronic structure with more positive charge character on iron upon oxidation. The polarization is supported by the Mössbauer data for **3**$^+$ PF$_6$$^-$, which indicate an iron(III) oxidation state.[10]

Also, ESR measurements show only 66% of the spin density on rhenium as compared to the dirhenium analogue **2**$^+$ PF$_6$$^-$. Table 5 predicts a reduction of 77%. Accordingly, the electronic structures of [**3-H**]$^+$ and **3**$^+$ PF$_6$$^-$ are best represented by the valence formulation ReC≡CC≡CFe$^{+\bullet}$. However, it is clear from the other data, including reduced IR $\nu_{C≡C}$ values,[28] that other resonance forms contribute.

Complex **3**$^+$ PF$_6$$^-$ exhibits an NIR band that has been assigned to an intervalence transition.[10] This has been interpreted as involving a less stable redox isomer best (but also not perfectly) represented by the valence formulation $^{+\bullet}$ReC≡CC≡CFe. As derived earlier, the energy difference can be approximated as 2904 cm^{-1} or 8.3 kcal/mol. However, the thermal energy barrier between these two species, which represent the limiting forms of a class II mixed valence compound, would be small. The computational modeling of such spin-crossover excited states is of interest, but due to various challenging aspects is outside the scope of the present study.

The dication [**3-H**]$^{2+}$ was examined next. As in the diiron series, the singlet [**3-H(S)**]$^{2+}$ and triplet [**3-H(T)**]$^{2+}$ were found to be essentially isoenergetic. Now the singlet was 1.9 kcal/mol more stable, a value which is within the limit of accuracy of the method used. This is in agreement with the magnetic susceptibility data for **3**$^{2+}$ 2PF$_6$$^-$. These establish a singlet ground state and a very low lying triplet excited state (0.35 kcal/mol) that is appreciably populated at room temperature.[10] Accordingly, **3**$^{2+}$ 2PF$_6$$^-$ is also ESR active. In any event, in the series [**1-H**]$^{2+}$, [**3-H**]$^{2+}$, and [**2-H**]$^{2+}$, the calculated singlet → triplet energy gap monotonically shifts from −1.9 to +1.9 to +8.1 kcal/mol. The corresponding energy difference for the diruthenium compounds [**5-H**]$^{2+}$ is +2.3 kcal/mol.[14] This trend can be related to the HOMO−LUMO gap found for the singlet state configuration of those dicationic compounds, which monotonically shifts from 0.17 to 0.38 eV to 0.78 eV, respectively.

The bond lengths in [**3-H(S)**]$^{2+}$ and [**3-H(T)**]$^{2+}$ (Table 8) differ more than in the homometallic singlets and triplets. With the singlet [**3-H(S)**]$^{2+}$, bond lengths and orders (Table 9) clearly indicate a cumulenic carbon chain. It is somewhat polarized, with higher bond orders for Re$-$C$_\alpha$ than Fe$-$C$_\alpha$ (1.265 vs 1.045) and C$_\alpha$$-C_\beta$ than C$_{\alpha'}$$-C_{\beta'}$ (2.020 vs 1.927). However, both M$-$C$_\alpha$ values are very close to those of the homometallic singlets. With the triplet [**3-H(T)**]$^{2+}$, C$_\alpha$$-C_\beta$ and C$_{\alpha'}$$-C_{\beta'}$ exhibit considerably more triple bond character (2.184 and 2.324), especially in the latter linkage, which is bound to iron. Table 5

Table 10. B3LYP Computed Adiabatic Ionization Potentials (eV) for Models [**1-H-3-H**]$^{n+}$, and Redox Potentials (V vs SCE, in Brackets) for **1**−**3**$^{n+}$ nX$^-$ and **6**$^{n+}$ nX$^-$

complex	$n=0$	$n=1$	$n=2$	$n=3$
[**1-H**]$^{n+}$	4.75	8.44	11.60	15.79
1^{n+} nX^{-} ^{a}	[−0.69]	[0.03]	[0.95]	
6^{n+} nX^{-} ^{b}	[−0.97]	[−0.18]	[0.81]	
[**2-H**]$^{n+}$	5.19	8.65		
2^{n+} nX^{-} ^{a}	[0.01]	[0.54]		
[**3-H**]$^{n+}$	4.79	8.52		
3^{n+} nX^{-} ^{a}	[−0.50]	[0.23]	[1.33]	

^{a} Reference 10. ^{b} Reference 11.

shows that the unpaired electrons are extensively delocalized. As with the monocation [**3-H**]$^+$, the highest spin density is found on iron, more than twice that as on rhenium. This spin density is also much greater than that found per iron in the symmetrical diiron analogue [**1-H(T)**]$^{2+}$. In summary, the electronic structures of [**3-H(S)**]$^{2+}$ and [**3-H(T)**]$^{2+}$ are best described by the valence formulations given for the diiron and dirhenium analogues, but with distinctly more polarization.

6. Ionization Potentials. To better understand the direction of polarization in the heterobimetallic complexes [**3-H**]$^{n+}$, the adiabatic gas-phase ionization potentials of [**1-H-3-H**]$^{n+}$ were calculated from the energy differences between oxidation states. The results are summarized in Table 10. The diiron complexes [**1-H**]$^{n+}$ are more readily ionized than their dirhenium counterparts [**2-H**]$^{n+}$ (e.g., 4.75 vs 5.19 eV for $n = 0$). This reflects the more electron-releasing nature of an iron endgroup, which lacks a good π-accepting ligand. The heterobimetallic complexes [**3-H**]$^{n+}$ give intermediate values (4.97 eV for $n = 0$), indicating electronic communication between the endgroups.

Solution-phase oxidation potentials normally track gas-phase ionization potentials.[14,18] As summarized in Table 10, cyclic voltammetry data show the same trend. The diiron complex **1** is 0.70 and 0.19 V thermodynamically easier to oxidize than the dirhenium and rhenium/iron complexes **2** and **3**. The above data show that the conversion of **3** to **3**$^+$ X$^-$ can be viewed as an iron-based oxidation. Hence, the replacement of an iron endgroup of **1** by a rhenium endgroup decreases the electron density at the remaining iron.

Conclusion

We have established that density functional calculations can reproduce the structural parameters of the real complexes [**1**−**3**]$^{n+}$ nPF$_6$$^-$, even if simplified models are used. The changes in geometrical structures of these neutral and cationic species are governed by the nodal properties of the highest MOs delocalized all over the metal and carbon atoms. In nearly all cases, spin states are also correctly predicted. This validates the computational method and the choice of model compounds and gives added confidence in cases where experimental data is not yet available.

In accord with all observed properties, the neutral complexes are best described by diynediyl or MC≡CC≡CM electronic structures, and the singlet dications are best described by cumulenic $^+$M=C=C=C=C=M$^+$ valence formulations. The latter clearly represents the electronic ground state for the dirhenium dication [**2-H**]$^{2+}$. However, the diiron and rhenium/iron dications [**1-H**]$^{2+}$ and [**3-H**]$^{2+}$ are calculated to possess triplet states of nearly identical energies, helping to clarify a considerable body of experimental data. The triplets have

dominant $^{\bullet+}$MC≡CC≡CM$^{+\bullet}$ character, but with some M−C$_\alpha$ multiple bonding and spin delocalization onto the carbon chain. This can be visualized with the resonance forms depicted for **Ic**-(**T**) in Scheme 4. The greater singlet/triplet energy gap for the dirhenium complex [**2-H**]$^{2+}$ is ultimately traceable to an enhanced energy difference between the HOMO and LUMO of its singlet state, disfavoring the triplet.

The mixed valence cation radicals [**1-H**–**3-H**]$^+$ also exhibit substantial delocalization of the unpaired electron, in accord with class III and class II assignments made from experimental data earlier. Although the electronic structures are best modeled by the resonance forms MC≡CC≡CM$^{+\bullet}$ ↔ $^{\bullet+}$MC≡CC≡CM, incipient M−C$_\alpha$ multiple bonding is evident. This can be visualized with the additional structures shown for **Ib** in Scheme 4. In the case of [**3-H**]$^+$, the odd electron is more heavily concentrated on iron than rhenium. In this context, the calculated adiabatic ionization potentials and experimental oxidation potentials clearly show the iron endgroup to be more electron rich. Accordingly, no dirhenium system has been oxidized beyond the dication stage.

For the iron trication [**1-H**]$^{3+}$, the B3LYP DFT data predict a quartet ground state. The electronic structure is best modeled by resonance forms that delocalize one of the three unpaired electrons onto the carbon bridge, as shown for **Id**-(**Q**) in Scheme 4. However, experimental data better fit a doublet ground state with a thermally accessible quartet excited state, in agreement with the BP86 DFT data. Since the doublet exhibits significant spin density on both the iron atoms and bridge, the electronic structure seems to comprise all of the resonance formulations depicted for **Id**-(**D**) in Scheme 4. For the iron tetracation [**1-H**]$^{4+}$, which to date has no real-molecule counterpart, a bis(carbyne) or $^{2+}$Fe≡CC≡CC≡Fe^{2+} electronic structure is predicted. The diruthenium complexes [**5-H**]$^{n+}$ and **5**$^{n+}$ nPF$_6$$^-$ are in most respects similar to the diiron complexes, except for the dications where singlet ground states are favored.

In summary, this study has highlighted the surprising diversity of electronic states that can be easily accessed energetically with carbon chain complexes [L$_m$MC$_4$M′L′$_n$]$^{z+}$.[5f] As emphasized earlier, every redox state in Scheme 2 can be expected to have unique physical and chemical properties, and many redox states feature low-lying excited electronic states with yet another set of properties. This provides a wealth of opportunities for utilizing such units to control and fine-tune electronic, magnetic, and charge communication in molecular devices. Now that the endgroup and redox dependence of these bonding and electronic structure properties has been addressed, the next frontier is clearly to study the effect of chain length and analogues with other types of carbon-rich ligands. Progress toward these objectives will be reported in future publications.

Experimental Section

Crystal Structures.[31] The slow diffusion of a layer of ether into a CH$_2$Cl$_2$ solution of **1** gave ruby-red cubic crystals of **1**·CH$_2$Cl$_2$. The slow diffusion of a layer of pentane into a CH$_2$Cl$_2$ solution of **6**$^{3+}$ 3PF$_6$$^-$ gave dark blue parallelepipeds. X-ray data were collected as summarized in Table 1.[32] Cell constants and an orientation matrix were obtained from a least-squares refinement using 25 high-θ reflections. Lorentz,

(31) Complexes **1** and **6**$^{3+}$ 3PF$_6$$^-$ were synthesized as reported earlier.[9,11]
(32) Spek, A. L. *HELENA. Program for Handling of CAD4-Diffractometer Output SHELX(S/L)*; Utrecht University: Utrecht, The Netherlands, 1997.

polarization,[33] and absorption corrections (ψ scans)[34] were applied. The structure was solved with SIR-97.[33] The parameters were refined with all data by full-matrix least-squares on F^2 using SHELX-93.[35] Non-hydrogen atoms were refined with anisotropic thermal parameters. The hydrogen atoms were fixed in idealized positions using a riding model. Scattering factors were taken from the literature.[36] Since the structure of **6**$^{3+}$ 3PF$_6$$^-$ has been communicated, only data for **1**·CH$_2$Cl$_2$ is provided in the Supporting Information.

Computations. Extended Hückel[37] studies of $\{(\eta^5\text{-}C_5H_5)(\eta^2\text{-}H_2PCH_2\text{-}CH_2PH_2)_2Fe\}_2C_4$ (**1-H**), $\{(\eta^5\text{-}C_5H_5)(NO)(PH_3)Re\}_2C_4$ (**2-H**), and $(\eta^5\text{-}C_5H_5)(\eta^2\text{-}H_2PCH_2CH_2PH_2)_2FeC_4Re(PH_3)(NO)(\eta^5\text{-}C_5H_5)$ (**3-H**), or their PH$_3$ analogues, were conducted with the program CACAO.[38] In other computations, geometries of [**1-H**−**3-H**]$^{n+}$ were fully optimized at the spin-unrestricted B3LYP hybrid density functional level of theory with the LANL2DZ basis set and an additional set of polarization functions as introduced by Hay and Wadt[39] and implemented in the Gaussian 98 program.[40] Frequency calculations were carried out at the same level to characterize the nature of the optimized geometries. For comparison, spin-unrestricted DFT calculations were also carried out using the ADF program with the BP86 functional and Slater basis sets.[41] Unless specified, comparable results were obtained. When needed, calculations using the broken-symmetry formalism[42] were carried out to compare valence-delocalized and presumably valence-localized geometries. The natural charges, bond orders, and population analysis were calculated using the NBO program.[43] The total electronic energies are given in the Supporting Information.

Supporting Information Available: Tables of calculated total electronic energies and coordinates for optimized geometries for [**1-H**−**3-H**]$^{n+}$ and crystallographic data for **1**·CH$_2$Cl$_2$. This material is available free of charge via the Internet at http://pubs.acs.org.

JA034619N

(33) Altomare, A.; Burla, M. C.; Camalli, G.; Cascarno, G.; Giacovazzo, C.; Guagliardi, A.; Moliterni, A. G. G.; Polidori, G.; Spagna, R. L. *J. Appl. Cryst.* **1998**, *31*, 74.

(34) Spek, A. L. *PLATON-98. A Multipurpose Crystallographic Tool*; Utrecht University: Utrecht, The Netherlands, 1998.

(35) Sheldrick, G. M. *SHELX-93. Program for Refinement of Crystal Structures*; University of Göttingen: Germany, 1993.

(36) Reidel, D. *International Tables for X-ray Crystallography*; Kynoch Press: Birmingham, 1974; Vol. IV.

(37) Hoffmann, R. *J. Chem. Phys.* **1963**, *39*, 1397.

(38) Mealli, C.; Proserpio, D. *J. Chem. Educ.* **1990**, *67*, 399.

(39) (a) Hay, P. J.; Wadt, W. R. *J. Chem. Phys.* **1985**, *82*, 299. (b) Dunning, T. H., Jr.; Hay, P. J. In *Modern Theoretical Chemistry*; Schaefer, H. F., III, Ed.; Plenum: New York, 1976; p 1. For polarization functions, see: Huzinaga, S.; Anzelm, J.; Klobukowski, M.; Radzio-Andzelm, E.; Sakai, Y.; Tatewaki, H. *Gaussian Basis Sets for Molecular Calculations*; Elsevier: Amsterdam, 1984.

(40) Frisch, M. J.; Trucks, G. W.; Schlegel, H. B.; Scuseria, G. E.; Robb, M. A.; Cheeseman, J. R.; Zakrzewski, V. G.; Montgomery, J. A., Jr.; Stratmann, R. E.; Burant, J. C.; Dapprich, S.; Millam, J. M.; Daniels, A. D.; Kudin, K. N.; Strain, M. C.; Farkas, O.; Tomasi, J.; Barone, V.; Cossi, M.; Cammi, R.; Mennucci, B.; Pomelli, C.; Adamo, C.; Clifford, S.; Ochterski, J.; Petersson, G. A.; Ayala, P. Y.; Cui, Q.; Morokuma, K.; Malick, D. K.; Rabuck, A. D.; Raghavachari, K.; Foresman, J. B.; Cioslowski, J.; Ortiz, J. V.; Stefanov, B. B.; Liu, G.; Liashenko, A.; Piskorz, P.; Komaromi, I.; Gomperts, R.; Martin, R. L.; Fox, D. J.; Keith, T.; Al-Laham, M. A.; Peng, C. Y.; Nanayakkara, A.; Gonzalez, C.; Challacombe, M.; Gill, P. M. W.; Johnson, B.; Chen, W.; Wong, M. W.; Andres, J. L.; Gonzalez, C.; Head-Gordon, M.; Replogle, E. S.; Pople, J. A. *Gaussian 98*, revision A.5; Gaussian, Inc.: Pittsburgh, PA, 1998.

(41) *Amsterdam Density Functional (ADF) Program*, releases 2.3 and 2000.02; Vrije Universteit: Amsterdam, The Netherlands, 1997, 2000. For computational method and applications, see: (a) Baerends, E. J.; Ellis, D. E.; Ros, P. *Chem. Phys.* **1973**, *2*, 41. (b) te Velde, G.; Baerends, E. J. *J. Comput. Phys.* **1992**, *99*, 84. (c) Fonseca Guerra, C.; Visser, O.; Snijders, J. G.; te Velde, G.; Baerends, E. J. In *Methods and Techniques for Computational Chemistry*; Clementi, E., Corongiu, G., Eds.; STEF: Cagliari, 1995; p 305.

(42) (a) Noodleman, L.; Norman, J. G., Jr. *J. Chem. Phys.* **1979**, *70*, 4903. (b) Noodleman, L. *J. Chem. Phys.* **1981**, *74*, 5737. (c) Noodleman, L.; Case, D. A. *Adv. Inorg. Chem.* **1992**, *38*, 423.

(43) (a) Glendening, E. D.; Reed, A. E.; Carpenter, J. E.; Weinhold, F. *NBO Programm, 3.1* as implemented in link 607 of Gaussian 98. (b) Reed, A. E.; Curtiss, L. A.; Weinhold, F. *Chem. Rev.* **1988**, *88*, 899.